A Study on the Distinguishing Responses of Shrinkage and Warpage to Processing Conditions in Injection Molding

Fen Liu, Shengqu Zeng, Huamin Zhou, Jianhui Li

State Key Laboratory of Material Processing and Die & Mold Technology, Huazhong University of Science and Technology, Wuhan 430074, People's Republic of China

Received 19 September 2010; accepted 1 September 2011
DOI 10.1002/app.35564
Published online 27 December 2011 in Wiley Online Library (wileyonlinelibrary.com).

ABSTRACT: A challenging task in injection molding industry is to minimize shrinkage and warpage (S&W) through optimal setting of molding conditions. In determining the relationship between molding conditions and product dimension, most existing literature considered S&W as a whole entity or focused on only one of them. The intention of this study was to distinguish these two terms, and perform a thorough analysis on the effect of operative conditions on S&W during injection molding process through a combination of experimental and numerical methods. Six process parameters with five levels were examined on a box-shaped product, and the single factor analysis of variance (ANOVA) was adopted in identifying the significance of each variable in the experiment. Results indicated that the effect of processing conditions on shrinkage is different from that on warpage. Specifically, packing pressure affects shrinkage most while packing time is the dominant factor in determining warpage. The reaction of shrinkage to packing pressure is monotonic, whereas the plot of warpage shows a U-shaped variation. A differential treatment of S&W can therefore help to enhance product quality. © 2011 Wiley Periodicals, Inc. J Appl Polym Sci 125: 731–744, 2012

Key words: injection molding; processing; poly(propylene); ANOVA

INTRODUCTION

As one of the most widely employed methods in polymer manufacture, injection molding often includes three stages: filling, packing, and cooling. During the filling stage, molten polymer is injected into the mold and fills the cavity. Once touching the mold wall, polymer starts cooling leading to shrinkage. Extra polymer melt is then introduced to compensate for the shrinkage during the packing stage. When the polymer solidifies to form the final shape, the product is ejected at the end of the cooling stage. During these processes, cooling and pressure effects will cause shrinkage, and differential shrinkage at different locations throughout a part eventually results in warpage.

Defined as the deviation from the mold geometry,[1] shrinkage concerns the dimensional difference from mold, whereas warpage regards more with deviation from the designed form. These two factors will deteriorate the dimensional stability of products. As final dimensions and geometry of a product is already a major quality criterion in modern industry, reducing shrinkage and warpage (S&W) has become a challenging task. Typically, S&W can be minimized by an appropriate setting of molding parameters (such as melt temperature, injection velocity, packing pressure, etc). As these process variables often have profound impacts on the final quality of products, their effect on S&W has therefore been a primary concern in injection molding industry.

A basic approach of studying parameter effects on S&W is setting several levels for a parameter, and a simple variation of S&W with the parameter can be obtained by comparing the S&W at each particular condition. Obviously, interaction effects of factors are ignored in this case. A number of researchers have conducted the experimental study in this way.[2–8] For example, Jansen et al.[3] measured the shrinkage of several amorphous and semicrystalline products from a rectangular cavity, and found that holding pressure was the key parameter, followed by the melt temperature. A recent study by Kurt et al.[6] employed a three-dimensional optical scanner system to measure the shrinkage of produced products without marking on the part surface. Kurt et al.

Correspondence to: H. Zhou (hmzhou@hust.edu.cn).
Contract grant sponsor: National Natural Science Foundation Council of China; contract grant number: 50875095.
Contract grant sponsor: National High-tech R&D Program of China (863 Program); contract grant number: 2009AA03Z104.

also agreed that packing pressure and melt temperature were the dominant factors in determining shrinkage. With a technique based on strain gauges, De Santis et al.[8] measured the transient shrinkage history of an iPP rectangular slab as a function of the holding pressure, and confirmed that shrinkage decreased with the increasing of holding pressure and time.

Many research groups have also worked in the numerical simulation of this area, and developed various mathematic models.[2,3,9–12] For example, Bushko and Stokes[11] modeled the product shrinkage from the solidification of a molten layer of thermoplastic between cooled parallel plates. They reported that the thickness shrinkage was affected by the processing parameters more than the in-plane shrinkage. Kwon et al.[13–15] found that the compressibility contribution to anisotropic shrinkage due to the solidification pressure was negligible, and added an elastic recovery term to the total shrinkage. Their simulation seemed to be in fair agreement with experimental result, which identified the packing time and packing pressure as the most important affecting parameters. For calculating warpage, Kabanemi et al.[16] employed a finite element method based on the theory of shells as an assembly of flat elements. Their simulation and experimental results on a PC box showed that a higher melt temperature produced a larger warpage, whereas an increasing cooling time decreased it. Similar numerical method for warpage simulation was also adopted by Zhou and Li.[17]

A clear understanding of the intrinsic relationship between S&W and processing conditions, however, cannot be achieved from above simple approaches, and requires a more scientific research planning, such as the design of experiments (DOE),[18–24] or a statistic data analysis technique. A typical application of DOE was adopted by Kramschuster et al.[18] who grouped the S&W of a box-shaped product into one term, and conducted a 2^{6-1} fractional factorial DOE. Analyzing the main and two-factor interaction effects statistically, they identified packing pressure and packing time as the most significant variables.

The most widely employed technique in data analysis, so far, may be the analysis of variance (ANOVA). A dramatic example from Chang and Faison[19] adopted a Taguchi method (a simplified DOE method) to illustrate the shrinkage changes with the variation of each processing parameter, and performed ANOVA to estimate the contribution of each factor to the whole response. Their study found that the significance of these molding parameters was different for each plastic. Following a similar approach, Wang et al.[20] observed that packing pressure was the most important factor on the warpage of a thin-walled part. Similar findings were reported by Liao et al.,[22] who measured S&W of a cellular phone's cover by the Cyclone Scanner, PolyCAD, and PolyWorks based on L-27 experimental tests. Their work was novel in studying both the shrinkage and warpage on the same product, and analyzing the effect of processing conditions on each of them. A recent ANOVA test of shrinkage by Altan[24] demonstrated that the most significant parameters for the PP and PS moldings were packing pressure and melt temperature, respectively. Using finite element analysis results of warpage based on the ANOVA, Ozcelik and Erzurumlu[25] identified the most influential parameter on the warpage of PC/ABS material was packing pressure. Similar application of ANOVA was reported with other materials.[26]

From the above review, it is clear that the conventional approach of studying S&W is superior in being simple and easy to perform, whereas the DOE provides more information but the procedure is a bit sophisticated. In addition, the ANOVA could serve as an effective tool in determining effects of process parameters.

Another more important point to make is that although a rich literature exists on the effect of processing conditions on S&W, most of the research focuses on only one term, either shrinkage[1–6,8,11,13,14,19,21,23,24,27,28] or warpage,[7,9,10,16,17,20,25,26,29–33] or regard them as a whole entity.[18] As a result, little work has been conducted on the different response of these two terms to the processing conditions. Does shrinkage react to processing parameters in the same way with warpage? The reality is, however, the mechanisms affecting shrinkage or warpage are quite different during the injection molding process[22]: the shrinkage is mainly attributed to an increase of density, and therefore a drop in volume when resins inside the mold cools down, while warpage is more concerned with the out-of-plane deformation resulting from the differential shrinkage or variations in shrinkage throughout the part.[34] A distinguishing characterization and treatment of S&W is therefore required in the optimal setting of molding conditions.

This study is aimed at distinguishing S&W behaviors on a box-shaped product, and uncovering the relationship between processing conditions and these two items through a combination of numerical and experimental methods. Six variable factors with five levels were studied, and the single factor ANOVA method was adopted in identifying the importance of each variable in the injection molding process.

RESEARCH DESIGN

For a worst-case study, a typical semicrystalline polymer, PP (F401, produced by PetroChina Co), was selected, as it is widely recognized that semicrystalline polymers shrink more compared with

TABLE I
Material Data for the PP

Material data	Value
Young's modulus (Mpa)	1340
Shear modulus (Mpa)	481.3
Poisson's ratio	0.392
Specific heat (liquid state) (J/kg K)	2740
Specific heat (glassy state) (J/kg K)	6860
Thermal expansion coefficient (K^{-1})	9.05×10^{-5}
Thermal conductivity (W/m K)	0.164

amorphous materials due to a closer packing of crystalline structure.[19] The material data for PP are listed in Table I.

Experimental setup

In most relevant studies, rectangular plates or bars were chosen,[2,3,8,10,17,19,24] which simplified the investigation process but ignoring the geometry effect. A box shape was considered to demonstrate the geometry effect as shown in Figure 1, with a dimension of $160 \times 100 \times 30$ mm^3 and a uniform wall thickness of 2.5 mm. A sprue gate was adopted in the center of the bottom surface. Two pressure transducers were mounted in the cavity, which left corresponding marks on the molded product referred to as P1 and P2. The experiment was performed on a 90-ton HTL90-F5B injection molding machine (manufactured by HAITAI Co, China).

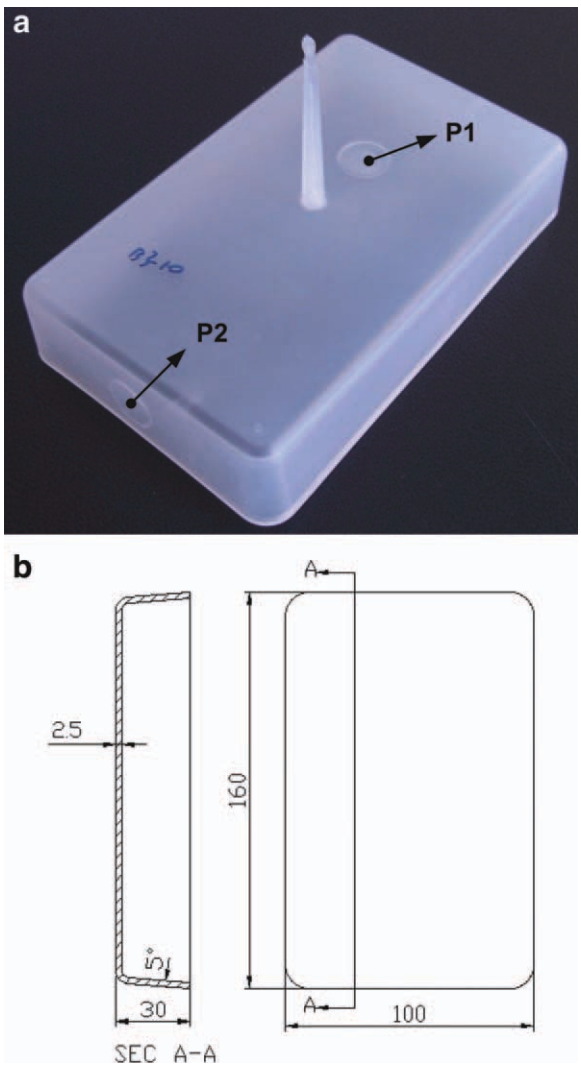

Figure 1 Schematic of a box-shaped product: (a) photo; (b) CAD graph. [Color figure can be viewed in the online issue, which is available at wileyonlinelibrary.com.]

TABLE II
Experimental Design for the Injection Molding Test

Factors	Symbols used in the study	Levels				
Melt temperature (°C)	A	220	230	240	250	260
Injection velocity (cm^3/s)	B	29	36	43	50	56
Mold temperature (°C)	C	30	40	50	60	70
Packing pressure (Mpa)	D	13	23	33	43	53
Packing time (s)	E	5	8	11	14	17
Cooling time (s)	F	3	6	9	12	15

Six process parameters were examined to study their effect on S&W, with five levels of settings shown in Table II. When the effect of one factor was evaluated, a random molding sequence was employed at its different levels, and the other five factors would adopt the standard setting as underlined in Table II. It should be pointed out that the cooling time was defined as the time from the end of packing stage toward ejection. The maximum and minimum settings of all process parameters were

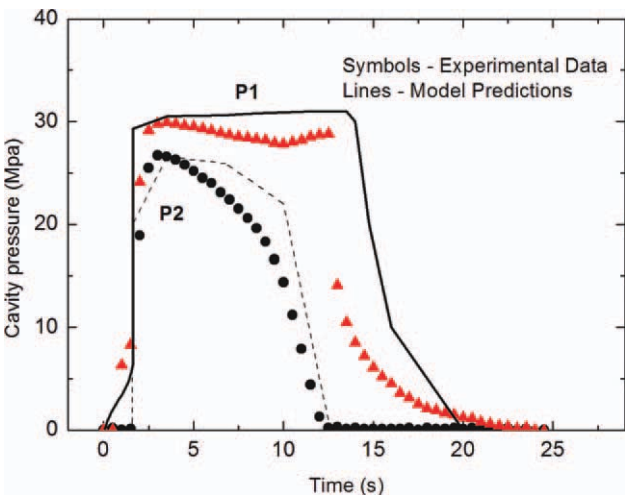

Figure 2 Experimental and simulated pressure curves for 'standard' sample. P1 and P2 indicate the position of pressure transducers as shown in Figure 1: P1 near the gate, P2 inside the cavity, 80 mm from the gate. [Color figure can be viewed in the online issue, which is available at wileyonlinelibrary.com.]

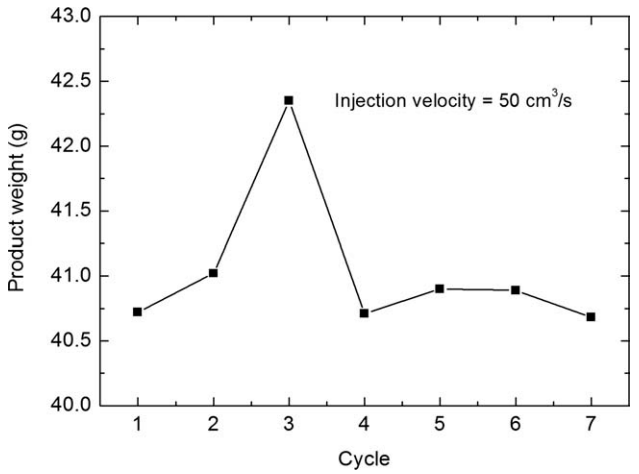

Figure 3 Cyclic change of the product weight as the injection velocity varies

determined through previous numerous experiments, which could generate a process window as large as possible, and also ensure the normal production of a qualified part. For example, the effective packing time levels were determined based on the cavity pressure measurement versus time as shown in Figure 2. The standard processing condition was adopted: melt temperature 240°C, injection velocity 43 cm^3/s, mold temperature 50°C, packing pressure 33 Mpa, packing time 11 s, cooling time 12 s. It can be seen that when the mold fills up with polymer, there is a moderate increase in pressure. Once the mold is full at about 2 s, packing stage begins and the pressure shoots up when additional material is forced into the cavity to compensate for the shrinkage caused by the increase of density. Finally, after gate freezing, the cooling stage starts and the pressure collapses in the form of a progressive pressure reduction. As it is commonly accepted that the effective packing time duration should be controlled by the gate freezing time, which in our case is about 13 s (11–12 s from the end of filling stage) as shown by the pressure curve of P1, different levels of packing time were set with a standard level around the gate freezing time, to study the effects of packing time duration before and after the gate freezing. It should also be noted that possible backflow may occur at the end of the packing phase especially when the packing duration is lower than the time to freeze. Effect of such backflow will be discussed later.

Steady condition test

As an essential step for accurately representing the characteristics of each processing parameter, a steady condition test was performed before the data collection, in order to ensure that samples are obtained under a steady processing condition. The product weight under different injection velocities was monitored to help determining the minimum cycles required before the steady condition is attained. Figure 3 shows the cyclic change of the product weight, when the injection velocity changes from 36 cm^3/s to 50 cm^3/s, with all the other parameters remaining standard.

It is clear that the weight curve of the box becomes flat from the forth cycle after the injection velocity changes. Samples collected after this cycle can therefore demonstrate the effect of a certain steady condition.

Measurement

A reference coordinate system was built as shown in Figure 4, with X and Y direction consistent with the length and width direction of the box, respectively. Four marks were machined on the four corners of the cavity (the marks were 140 mm apart in length

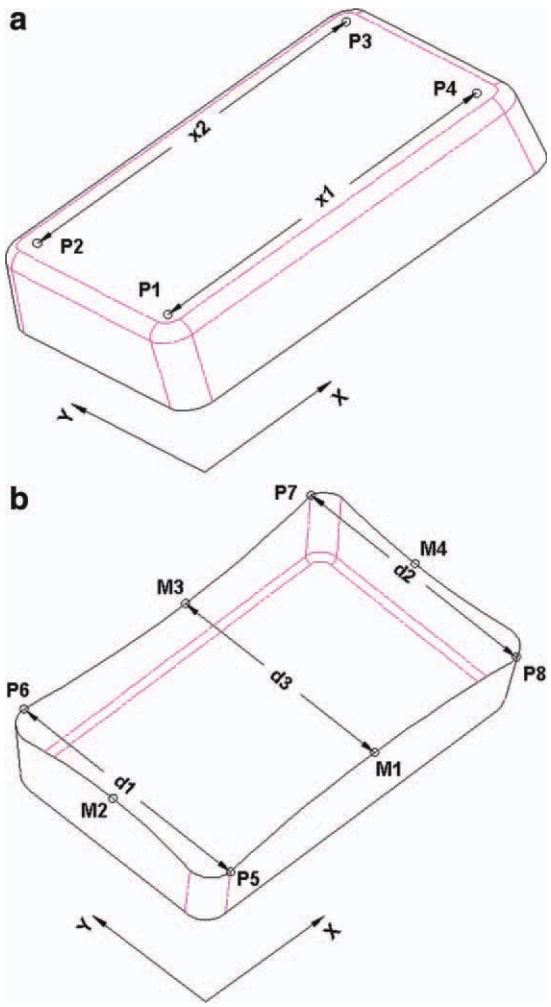

Figure 4 Schematic of measurement: (a) shrinkage; (b) warpage. [Color figure can be viewed in the online issue, which is available at wileyonlinelibrary.com.]

TABLE III
7-Constant Model Constants for the PP Used in Simulations

Symbol	ñ	τ* (Pa)	D_1 (Pa s)	D_2 (K)	D_3 (K/Pa)	A_1	A_2 (K)
Value	0.2796	27800	1.89×10^{12}	263.15	0	25.067	51.6

and 80 mm apart in width direction), which left corresponding markings on the bottom surface of the box after molding shown as P1, P2, P3, and P4. Let x_1 and x_2 represent the distances between the two markings in the X direction of the product, the experimental x-direction shrinkage was defined by the dimensional deviation of product from the cavity as:

$$S_x = \frac{1}{2}(\Delta x_1 + \Delta x_2) = \frac{280.0 - (x_1 + x_2)}{140.0} \quad (1)$$

where Δx_i, $i = 1,2$: shrinkage of the x_i segment. A similar definition was applied to the y-direction shrinkage.

Defining four corner points on the side wall as P5 to P8, and the midpoints as M1 to M4, the y-direction warpage could take the form:

$$W_y = \frac{1}{2}[(d_1 - d_3) + (d_2 - d_3)] \quad (2)$$

where d_1 and d_2 represent the distance between the corner points, and d_3 is the distance between the midpoints of M1 and M3 in Y direction. The x-direction warpage was described in a similar way.

A digital slide caliper (MITUTOYO (Japan) 500-197-20) was used for measurement. The same injection part was measured three times, and the average value was adopted, which minimized the measurement error and ensured the repeatability of the measuring procedure.

Data collection and analysis

A total of 10 products were molded for each condition, and the production sequence number from 1 to 10 was recorded as the label for each part. Samples numbered from 5 to 10 under the same condition were collected as a result of the previous steady condition test, which also reduced the impact of random error. These parts were placed in a dry and clean vessel under the room temperature for 30 days before the measurement.

TABLE IV
Specific-Volume Model Constants for the PP Used in Simulations

Symbol	Value	Symbol	Value
$b_{1,l}$ (m^3/kg)	0.001302	$b_{1,S}$ ((m^3/kg)	0.001213
$b_{2,l}$ (m^3/kg K)	9.919×10^{-7}	$b_{2,S}$ (m^3/kg K)	6.909×10^{-7}
$b_{3,l}$ (Pa)	6.767×10^{7}	$b_{3,S}$ (Pa)	8.922×10^{7}
$b_{4,l}$ (K^{-1})	0.003887	$b_{4,S}$ (K^{-1})	0.007946
b_5 (K)	443.15	b_6 (K/Pa)	3.701×10^{-8}

The single factor ANOVA method was adopted to evaluate the contribution of each factor to S&W, which was shown by the F-value in a typical ANOVA table. The significance of a single factor to the whole response was described by the P-value. With $P \leq 0.1$, an evident impact of the factor could be assumed. The 95% confidence interval was employed to check the distribution of the data. The above analysis was performed with the data analysis software Minitab.

Numerical simulation

A numerical simulation of injection molding process was also performed. Before the S&W analysis, the injection molding cycle should be simulated in order to obtain the initial temperature and pressure fields. Pressure and temperature history throughout the part was calculated from the constitutive equations of mass, momentum and energy, with specific assumptions and boundary conditions for each particular stage. For example, the governing equations for the filling stage are written as[35–37]

$$u_{i,i} = 0 \quad (3)$$

$$2\eta\dot{\varepsilon}_{ij,j} - P_{,i}\delta_{ij} = 0 \quad (4)$$

$$\rho C_p(T_{,t} + u_i T_{,i}) = \frac{\eta}{2}(u_{i,j} + u_{j,i})^2 + KT_{,ii} \quad (5)$$

where $\dot{\varepsilon}_{ij} = \frac{1}{2}(u_{i,j} + u_{j,i})$; the symbol ',' denotes derivatives, $i = 1,2,3$ and $j = 1,2,3$ are the coordinate components; u, P and T are velocity, pressure, and temperature with η, ρ, C_p and K being dynamic viscosity, density, specific heat, and the thermal conductivity, respectively.

The basic assumptions for the filling stage can be given as: (a) melt is incompressible and purely viscous; (b) inertia force is neglected when compared with viscous force. In addition, the following boundary conditions were adopted: (a) the polymer will remain the mold temperature once it contacts the mold wall, therefore the heat resistance between the mold wall and polymer melt is neglected; (b) a nonslip condition applied during both filling and postfilling stage, i.e., the flow rate of the polymer at the mold wall is assumed zero.[35–37]

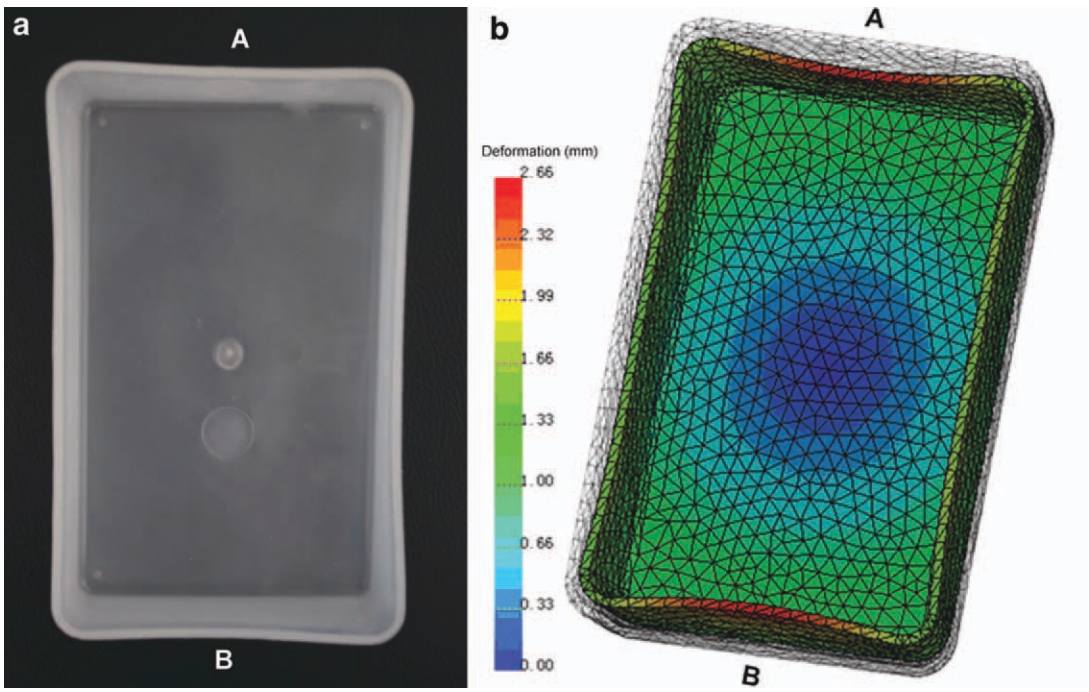

Figure 5 Deformation of the box under the standard processing condition: (a) experimental result; (b) simulation result. [Color figure can be viewed in the online issue, which is available at wileyonlinelibrary.com.]

The 7-Constant Cross-WLF model was employed to describe the rheological behavior of polymer melts, which follows:

$$\eta(T,\dot{\varepsilon}) = \frac{\eta_0(T,P)}{1+\left(\frac{\eta_0\dot{\varepsilon}}{\tau^*}\right)^{1-\tilde{n}}} \tag{6}$$

$$\eta_0 = D_1 \exp\left(\frac{-A_1(T-(D_2+D_3P))}{A_2+T-D_2}\right) \tag{7}$$

where $\dot{\varepsilon}$ is the shear strain rate, T and P representing the temperature and pressure, $\tilde{n}$ the power-law index, τ^* the shear constant, and A_1, A_2, D_1, D_2, D_3 are material constants obtained from the rheological measurement.

For the post-filling stage, the compressibility of the polymer was included in the model. The Tait equation was selected for illustrating the relationship between polymer density and processing conditions, which reads

$$\rho = \left[\nu_0\left(1 - C\ln\left(1+\frac{P}{B}\right)\right) + \nu_t\right]^{-1} \tag{8}$$

in which $C = 0.0894$, and

$$\nu_0 = \begin{cases} b_{1l} + b_{2l}(T-b_5) & T \geq T_g \\ b_{1s} + b_{2s}(T-b_5) & T < T_g \end{cases} \tag{9}$$

$$B = \begin{cases} b_{3l}e^{-b_{4l}(T-b_5)} & T \geq T_g \\ b_{3s}e^{-b_{4s}(T-b_5)} & T < T_g \end{cases} \tag{10}$$

$$\nu_t = \begin{cases} 0 & T \geq T_g \\ b_7 e^{b_8(T-b_5)-b_9P} & T < T_g \end{cases} \tag{11}$$

where T_g is the crystallizing point for crystalline materials, which can be written as $T_g = b_5 + b_6P$ and b_{1l}, b_{2l}, b_{3l}, b_{4l}, b_{1s}, b_{2s}, b_{3s}, b_{4s}, b_5, b_6, b_7, b_8, b_9 are material constants obtained from the PVT test. A 3D finite element model was applied to solve the nonisothermal, viscous, and non-Newtonian flow problem of injection molding in this article.[35] Detailed model constants used in simulations are outlined in Tables III and IV.

A linear thermoviscoelastic model was adopted for simulating thermally and pressure induced residual stresses. The stress in the packing and cooling stages was expressed as the combination of a hydrostatic stress and deviatoric components of stress[38,39]:

$$\sigma_{ij} = -P_h\delta_{ij} + \tau_{ij,} \quad i,j = 1,2,3 \tag{12}$$

where P_h is the hydrostatic stress or the negative value of stress spherical tensor, τ_{ij} denoting the deviatoric components of stress, and δ_{ij} is the kronecker delta. For isotropic materials, it follows:

TABLE V
A Comparison of S&W under the Standard Condition

Methods	S_x (‰)	S_y (‰)	W_x (mm)	W_y (mm)
Experiment	17.03	15.35	1.89	1.63
Simulation	17.17	15.98	2.17	1.41

TABLE VI
ANOVA Table for X-Direction Shrinkage

Factor	DOF	SS	MS	DOF of error	SS of error	MS of error	F-value	*P*-value
A	4	6.3175	1.5794	25	0.3562	0.0142	110.84	0.000
B	4	2.2086	0.552	25	0.4257	0.0170	32.4	0.000
C	4	14.0232	3.5058	25	0.6532	0.0261	134.18	0.000
D	4	584.732	146.183	25	1.0286	0.0411	3552.79	0.000
E	4	71.8073	17.9518	25	0.5335	0.0213	841.16	0.000
F	4	13.6255	3.4064	25	0.4501	0.0180	189.22	0.000

$$P_h = -\frac{1}{3}Tr\sigma = -\int_{-\infty}^{t} G_1(\xi(t)-\xi(t'))\left(\frac{\partial \varepsilon_m}{\partial t'} - \frac{\partial \varepsilon_{\text{th}}}{\partial t'}\right)dt' \quad (13)$$

$$\tau_{ij}(t) = \int_{-\infty}^{t} G_2(\xi(t)-\xi(t'))\frac{\partial \varepsilon_{ij}^d}{\partial t'}dt' \quad (14)$$

where G_1 and G_2 are the bulk and shear relaxation modulus functions;$Tr\sigma$ is the trace of the stress tensor σ_{ij};t and t' are time variables;$\xi(t)$ represents the pseudo-time; ε_m and ε_{ij}^d express the spherical and deviatoric components of strain tensors;ε_{th} is the thermal strain due to temperature changes. For each molding stage, boundary conditions were given as follows[32]:

1. During the packing stage, the normal stress σ_{33} was obtained from the cavity pressure in the packing analysis:

$$\sigma_{33} = -P \quad (15)$$

2. When the gate solidifies or packing stage completes, there would be no effect of packing pressure. However, the product would continue to attach closely to the mold surface under the cavity pressure, and geometry would not vary in the thickness direction.
3. During the cooling stage, the product was allowed to detach from the mold surface, and shrink in the thickness direction.
4. After demolding, the product was free from mold constraints. Warpage and deformation were induced with the release of residual stresses when the product was cooled to the room temperature.

It is clear that the above multiple boundary conditions could account for the impacts of packing stage and gate solidification on residual stresses.

The final S&W of the injection molded product were simulated based on the shell theory as an assembly of flat elements. Deformation of a typical flat element can be presented by the in-plane deformation of a membrane element combined with the bending deformation of a bending element.[7,10,16,17,28,29,32,33] Take a triangular flat element for example, with the commonly accepted linear thermal elastic model, the local equilibrium equation reads:

$$K^e q^e = r^e \quad (16)$$

where q^e and r^e are the integrated local nodal displacements and loads, and K^e is the integrated stiffness matrix, which submatrix is

$$K_{rs}^e = \begin{bmatrix} k_{11}^m & k_{12}^m & 0 & 0 & 0 & k_{13}^m \\ k_{21}^m & k_{22}^m & 0 & 0 & 0 & k_{23}^m \\ 0 & 0 & k_{11}^p & k_{12}^p & k_{13}^p & 0 \\ 0 & 0 & k_{21}^p & k_{22}^p & k_{23}^p & 0 \\ 0 & 0 & k_{31}^p & k_{32}^p & k_{33}^p & 0 \\ k_{31}^m & k_{31}^m & 0 & 0 & 0 & k_{33}^m \end{bmatrix} \quad (17)$$

where k_{ij}^m and k_{ij}^p are the corresponding elements of in-plane stiffness matrix K_m^e and bending stiffness matrix K_p^e, respectively. An optimal membrane triangular element (OPT element) with rotational degree of freedom proposed by Felippa[40] was adopted as the membrane element in current model, based on the technique of Assumed Natural DEviatoric Strain formulation (ANDES). And a triangular thin/thick

TABLE VII
ANOVA Table for Y-Direction Shrinkage

Factor	DOF	SS	MS	DOF of error	SS of error	MS of error	F-value	*P*-value
A	4	1.1657	0.2914	25	0.3167	0.0127	23.01	0.000
B	4	0.4826	0.1206	25	0.3761	0.0150	8.02	0.000
C	4	5.0169	1.2542	25	0.2727	0.0109	115.00	0.000
D	4	989.355	247.339	25	0.6290	0.0252	9831.17	0.000
E	4	91.9797	22.9949	25	0.4852	0.0194	1184.81	0.000
F	4	4.8119	1.2030	25	0.3111	0.0124	96.68	0.000

TABLE VIII
ANOVA Table for X-Direction Warpage

Factor	DOF	SS	MS	DOF of error	SS of error	MS of error	F-value	*P*-value
A	4	0.8462	0.2115	25	1.2496	0.0500	4.23	0.009
B	4	0.5197	0.1299	25	1.4902	0.0596	2.18	0.101
C	4	9.0791	2.2698	25	1.4997	0.0600	37.84	0.000
D	4	2.7434	0.6858	25	1.9924	0.0797	8.61	0.000
E	4	11.1133	2.7783	25	1.7270	0.0691	40.22	0.000
F	4	2.8962	0.7240	25	1.5265	0.0611	11.86	0.000

plate elements (RDKTM) based on the refined nonconforming element method (RNEM) was employed in current study as the bending element, which was developed by Chen and Cheung.[41] The above flat model was performed using surface mesh of products in S&W analysis,[32,42] which avoided the traditional troublesome work of midplane creation.

RESULTS AND DISCUSSION

Case study under the standard condition

A typical sample produced under the standard condition and corresponding simulated result are displayed in Figure 5. The simulated deformation (S&W) is presented with a scale factor of 10 for a clearer display. It can be seen that the four side walls of the box all shrink inward leading to the warpage of the product, and the most severe deformation seems to appear in the middle of the two shorter side walls (marked as A and B in the photo). These deformation trends are clearly shown by simulation results in Figure 5(b).

A detailed comparison of S&W is outlined in Table V. It is clear that simulated deformation is in fair quantitative agreement with the experimental result.

Single factor ANOVA result

The single factor ANOVA method was used to analyze the experimental data of S&W, and the results are outlined from Tables VI–IX.

As can be seen, all *P* values are well under 0.1, and the only exception is the response of x-direction warpage to the injection velocity which is slightly above 0.1. As has been said, a low value of *P* indicates an observable contribution of a factor to the whole quality, which means the six factors in study have a clear effect on S&W of the box-shaped product.

The F-value can be defined as the ratio of variance between items and variance within items, and the statistical significance of a factor can be tested by comparing the F-value. A larger F-value can often imply a greater effect of the control factor on the observed factors.[22] For current study, following order of influence can be obtained:

- *x*-direction shrinkage: D>E>F>C>A>B
- *y*-direction shrinkage: D>E>C>F>A>B
- *x*-direction warpage: E>C>F>D>A>B
- *y*-direction warpage: E>C>D>A>F>B

where A is the melt temperature, B, the injection velocity, C, the mold temperature, D, the packing pressure, E, the packing time, F, the cooling time.

It can be seen from the ANOVA analysis that packing pressure is the most important factor influencing the shrinkage, whereas packing time affects the warpage most. Although present analysis did not take into account the interactive effects of factors, the identification of the most important factor in affecting shrinkage still corresponded well with most relevant studies.[2,3,5] However, most previous research on warpage concluded the packing pressure as the most significant parameter,[20,30,43] probably due to different material properties and geometry effect. It also shows that the effect of injection

TABLE IX
ANOVA Table for Y-Direction Warpage

Factor	DOF	SS	MS	DOF of error	SS of error	MS of error	F-value	*P*-value
A	4	2.7427	0.6857	25	0.4227	0.0169	40.55	0.000
B	4	0.6829	0.1707	25	0.9244	0.0370	4.62	0.006
C	4	12.0566	3.0141	25	0.9733	0.0389	77.42	0.000
D	4	18.590	4.647	25	2.598	0.104	44.71	0.000
E	4	48.2675	12.0669	25	1.5532	0.0621	194.22	0.000
F	4	1.3699	0.3425	25	0.7094	0.0284	12.07	0.000

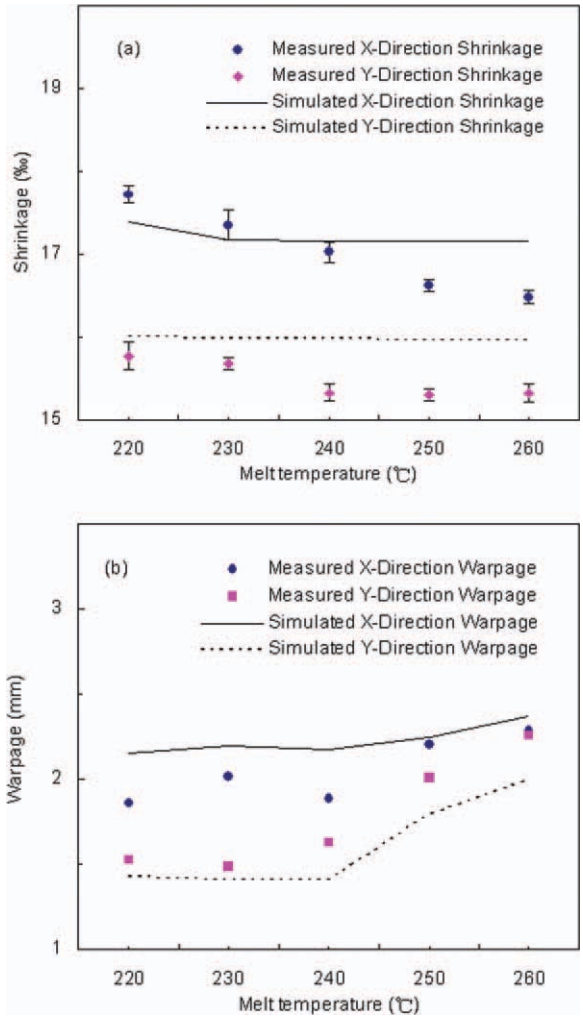

Figure 6 Measured and predicted S&W as a function of melt temperature: (a) shrinkage; (b) warpage. [Color figure can be viewed in the online issue, which is available at wileyonlinelibrary.com.]

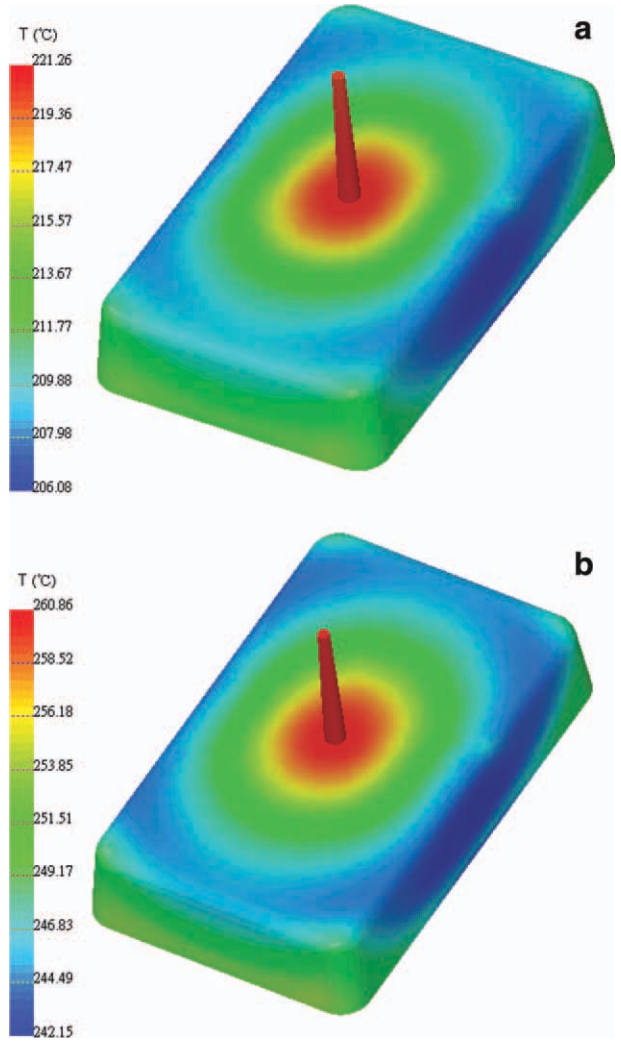

Figure 7 Predicted temperature fields at the end of filling stage with a melt temperature of: (a) 220°C; (b) 260°C. [Color figure can be viewed in the online issue, which is available at wileyonlinelibrary.com.]

velocity on either shrinkage or warpage seems to be the least significant.

Effect of processing conditions

To study the different reactions of S&W to process parameters, experimental and simulated S&W as a function of various processing parameters are plotted below. It should be noted that the experimental warpage data are the mean values (95% confidence) from the six samples produced under the same condition. Error bars have been reported on measured shrinkages which show good reproducibility of data.

As can be seen, shrinkages under all processing conditions fall within the range of 10 to 30‰. And the shrinkage of x-direction (which lies in the length direction of the part) is obviously higher than that of y-direction (which is also the width direction of the part) at all studied levels, probably due to different cooling rates from geometry effects. As for the pro-

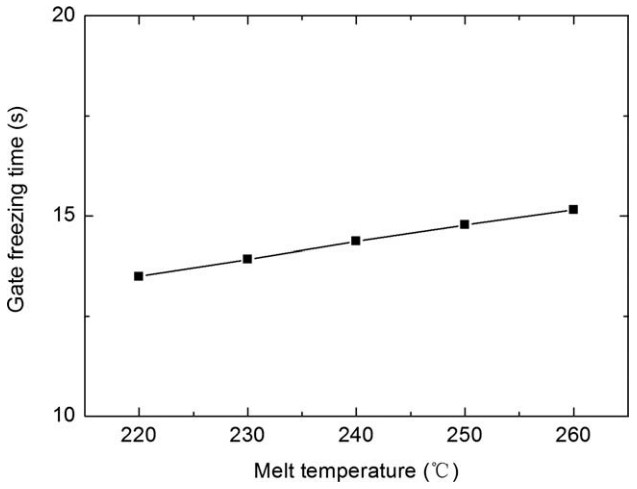

Figure 8 Predicted gate freezing time as a function of melt temperature

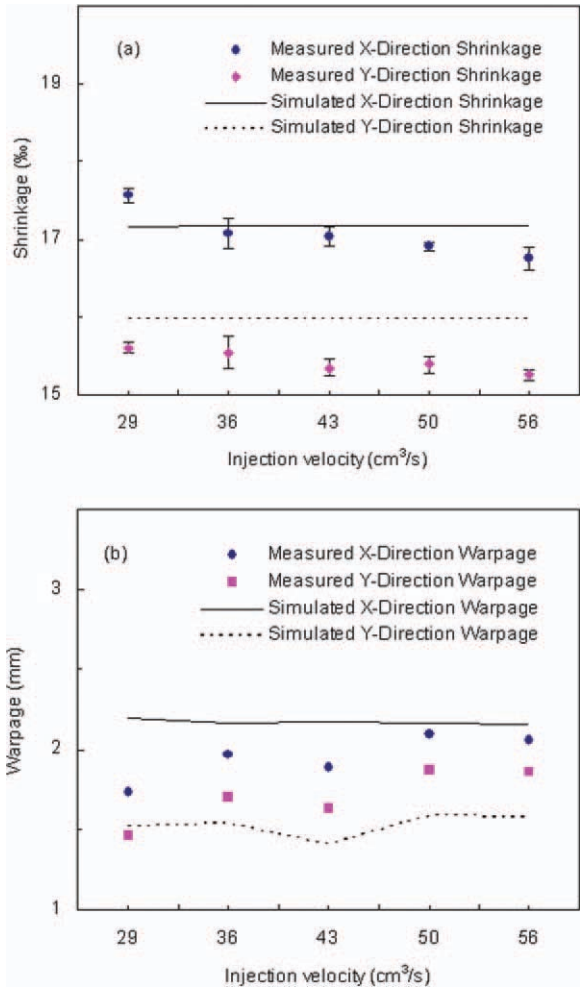

Figure 9 Measured and predicted S&W as a function of injection velocity: (a) shrinkage; (b) warpage. [Color figure can be viewed in the online issue, which is available at wileyonlinelibrary.com.]

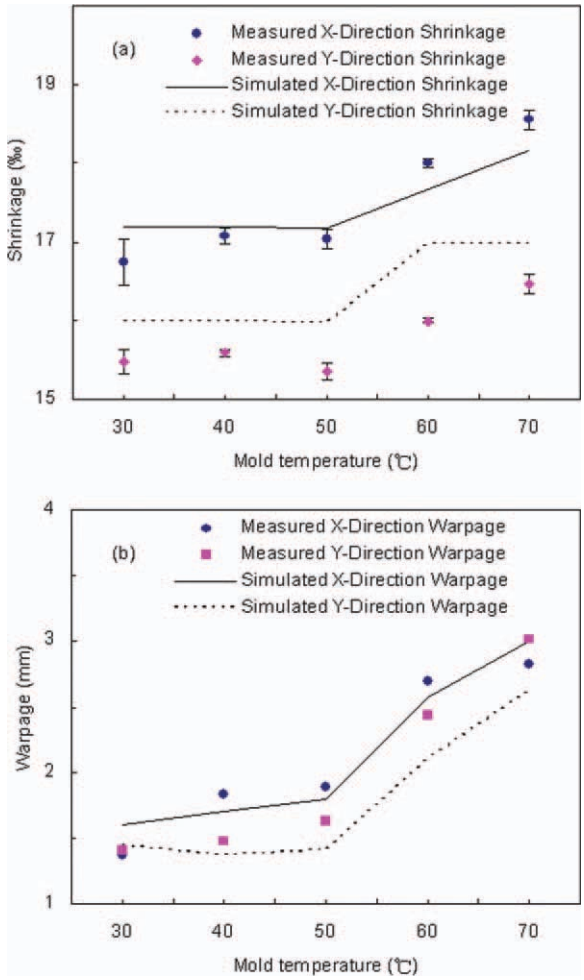

Figure 10 Measured and predicted S&W as a function of mold temperature: (a) shrinkage; (b) warpage. [Color figure can be viewed in the online issue, which is available at wileyonlinelibrary.com.]

files of warpage, all warpage values vary between 1.0 mm and 5.0 mm.

Effect of melt temperature

As shown by Figure 6, shrinkage shows a slightly declining response with melt temperature, whereas warpage can be enhanced with a higher melt temperature. With the increase of the melt temperature, gate areas will take higher temperatures at the end of filling as shown in Figure 7, and gate freezing is delayed as shown in Figure 8, allowing more polymers to enter the cavity and compensate for the volume shrinkage, which will reduce final shrinkage. On the other hand, a higher melt temperature means a larger difference between the melt and mold temperature, which will cause a higher thermal shrinkage after ejection. Final shrinkage is, therefore, the result of a competitive mechanism between these two effects.[13] As the side walls of the box appear to be more sensitive to the additional shrinkage caused by the cooling effect, the rise of melt temperature may therefore lead to a higher warpage depicted in

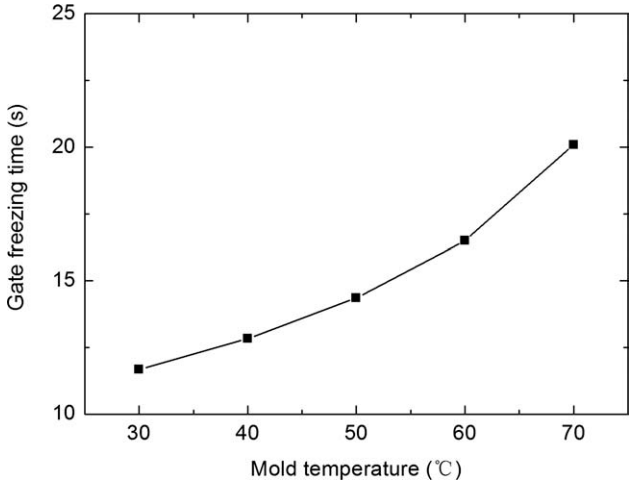

Figure 11 Predicted gate freezing time as a function of mold temperature

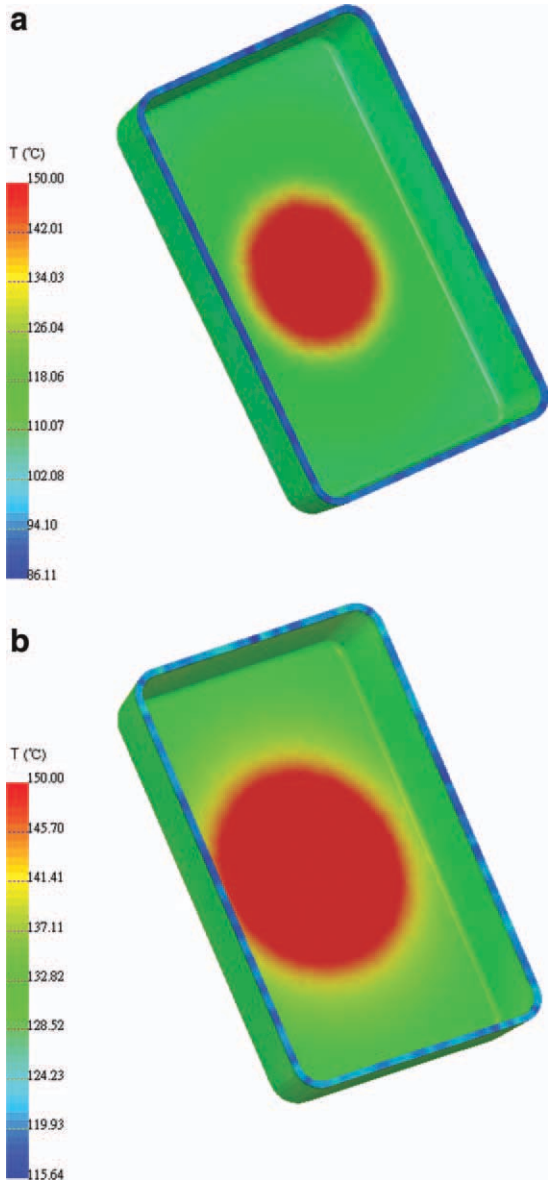

Figure 12 Predicted temperature fields at the end of packing stage with a mold temperature of: (a) 30°C; (b) 70°C. [Color figure can be viewed in the online issue, which is available at wileyonlinelibrary.com.]

Figure 6(b). The result of shrinkage versus melt temperature does not correspond with Kwon et al.,[13] and the geometry effect may well be the cause. In addition, a higher temperature shows in *x*-direction (the length direction of the part) than that of *y*-direction (the width direction of the part) at the end of filling stage in Figure 7, which may lead to a higher shrinkage in *x*-direction after the product cools down.

Effect of injection velocity

A similar response of S&W to the injection velocity was observed, suggesting an insignificant effect of injection velocity on final dimension as shown in Figure 9. Disagreements arise with Pomerleau and Sanschagrin[1] about the effect of injection velocity on shrinkage, probably due to the part geometry effect as different geometries were employed.

Effect of mold temperature

A clear effect of mold temperature on shrinkage and warpage is indicated in Figure 10. Although gate freezing time is longer at a higher mold temperature as shown in Figure 11, the additional cooling effect with a higher mold temperature (as shown in temperature fields at the end of packing stage in Figure 12, where the upper value of temperature for show has been limited to 150°C for a better comparison) would introduce a higher shrinkage,[13] and thus a larger warpage. As the side walls of the box will be more sensitive to the additional shrinkage caused by the cooling effect, warpage variation with the mold temperature appears more severe.

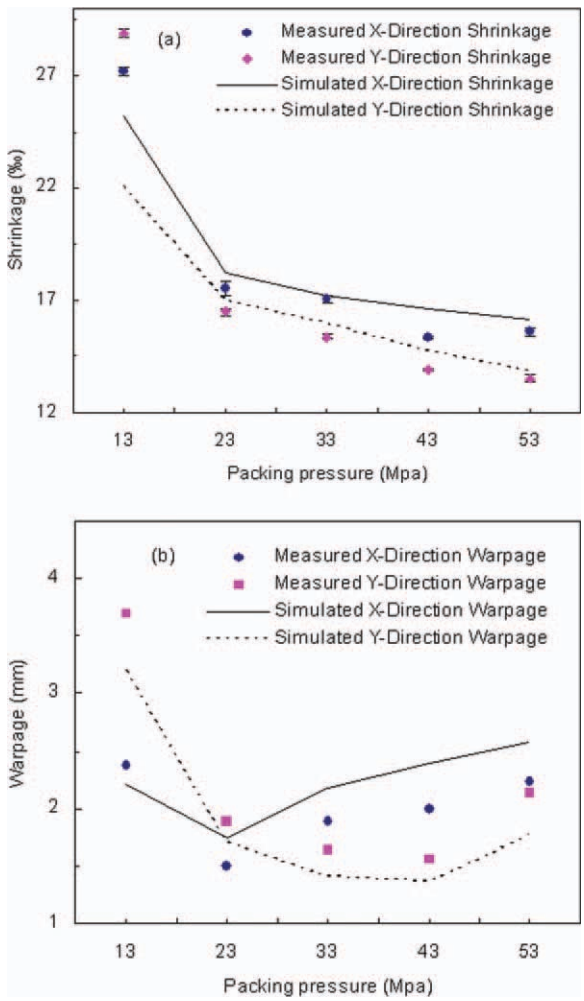

Figure 13 Measured and predicted S&W as a function of packing pressure: (a) shrinkage; (b) warpage. [Color figure can be viewed in the online issue, which is available at wileyonlinelibrary.com.]

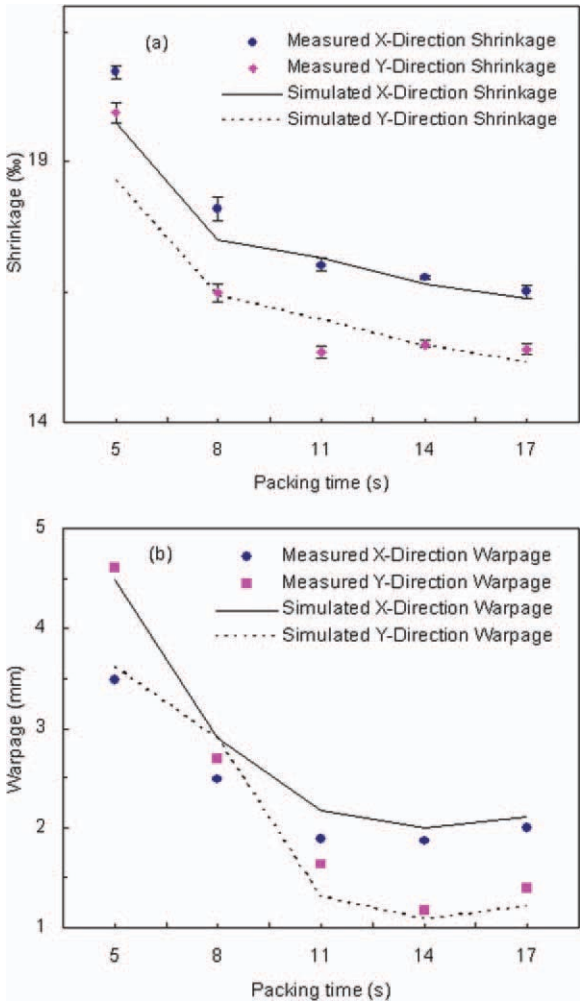

Figure 14 Measured and predicted S&W as a function of packing time: (a) shrinkage; (b) warpage. [Color figure can be viewed in the online issue, which is available at wileyonlinelibrary.com.]

Effect of packing pressure

It can be seen from Figure 13 that the effect of packing pressure on shrinkage is significant and negative, following most relative expectations,[3,5,8,18,20] while the reaction of warpage to packing pressure is not monotonic but shows a U-shaped variation instead. When the packing pressure is too low (such as 13Mpa in our case), backflow may occur around the gate at the end of packing phase, and the compensation effect of additional polymers during the packing stage can therefore be offset, leading to the increased S&W as packing pressure reduces. As packing pressure increases, warpage will fall down at first like shrinkage, due to the better compensation of additional materials and a reduced effect of possible backflow. When packing pressure rises above a certain level, higher residual stresses will be induced, resulting in a bigger warpage as in Figure 13(b). The shrinkage may not be affected much by the rise of residual stresses and continues to decrease as in Figure 13(a). Simulation results can well describe the effects of packing pressure on S&W, especially the U-shaped response of warpage, in spite of some quantitative deviations.

Effect of packing time

As plotted in Figure 14, a longer packing time will normally reduce the final S&W as the packing pressure does, mainly owing to the better compensation of polymers. It should also be noted that when the packing time duration exceeds 11 s, the variation of S&W becomes less distinctive, confirming our previous expectation that gate freezes around 11 s from the end of filling stage. It has long been realized that when the packing duration is lower than the time to freeze, runner system does not freeze before the part, leading to probable backflow. Such backflow may counteract the compensation during the packing stage, resulting in the increase of S&W as packing time shortens. As packing time extends after the gate

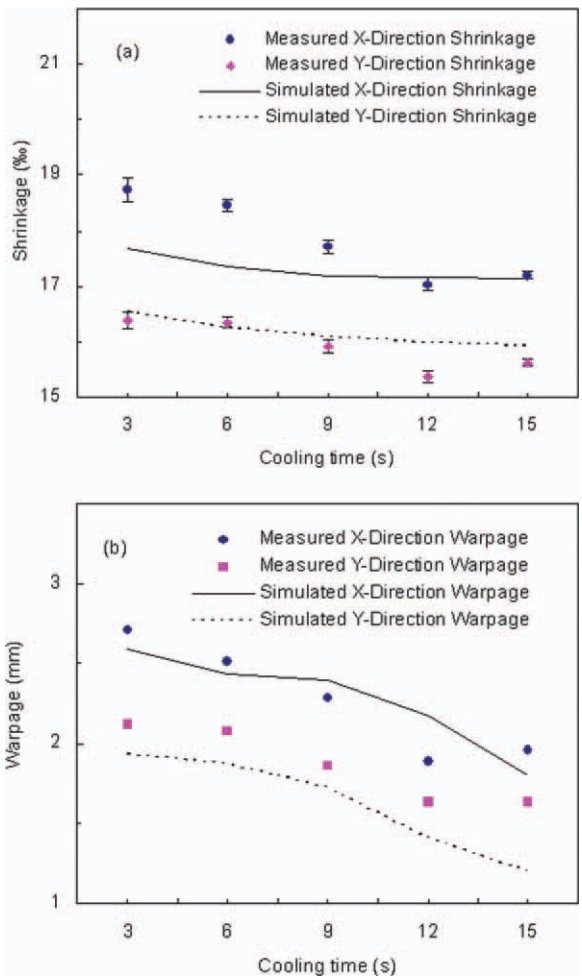

Figure 15 Measured and predicted S&W as a function of cooling time: (a) shrinkage; (b) warpage. [Color figure can be viewed in the online issue, which is available at wileyonlinelibrary.com.]

freezes, neither backflow nor compensation of additional polymers into the cavity becomes possible. Therefore, S&W will not change dramatically thereafter. Simulated shrinkage results change with packing time also for times longer than gate solidification, which may be attributed to the initial deviations of calculated pressure and temperature distribution of packing and cooling simulation. For example, the omission of heat transfer in the mold of current model may lead to an over-predicted temperature of polymer, which may in turn result in the delayed calculated gate solidification time as shown by Figure 2 (simulated gate solidification time of about 15 s compared with measured 13 s). This deviation will definitely underestimate the effect of gate solidification and influence the final simulated shrinkage results. For further improvement, the accuracy of simulated pressure and temperature results needs enhancing.

Effect of cooling time

It is clear from Figure 15 that cooling time does not have large effect on shrinkage, whereas a longer cooling time can reduce the warpage. Increased cooling time usually allows the residual stress to relax more before ejection, and this will lead to a lower warpage as in Figure 15(b). As shrinkage may not be so closely related to residual stresses, the effect of cooling time on it seems less pronounced [Fig. 15(a)].

CONCLUSIONS

The aim of this research was to examine differential responses of shrinkage and warpage to process parameters. A thorough analysis of the effect of operative conditions of injection molding process on both S&W was conducted.

Comparing the response of shrinkage with that of warpage when changing the same process parameter, it was found that shrinkage responded in a dramatically different way from warpage. Following observations can be made:

1. Warpage appears to react in a much more drastic way than shrinkage, probably due to a bigger deformation space available for the side walls of box after ejection;
2. The most important factor in determining shrinkage seems to be the packing pressure, whereas packing time may affect warpage most;
3. Although the reaction of shrinkage to packing pressure is monotonic, the warpage profile shows a U-shaped response.

From above results, it can be concluded that the optimum processing conditions for minimizing shrinkage or warpage may be quite different. For maximum effect of reducing shrinkage, a higher packing pressure with a longer packing time should be considered, whereas it is better to select appropriate packing condition along with lowering the additional cooling effect (melt or mold temperature etc) in order to minimize the final warpage.

A satisfactory qualitative agreement between model prediction and experimental data was exhibited, indicating the validity of current numerical simulations. Some quantitative differences can be observed, such as the simulated shrinkage response to the packing time, which may be attributed to the simplifications of the model. The most relevant factors may be the thermal simplifications. For example, the boundary condition of a perfect contact between the mold wall and polymer melt was used in the simulation. However, in a real process, the contact can never be perfect and heat resistance inevitably exists, the omission of which can lead to deviations in simulation results. For better prediction, heat transfer in the mold should be accounted for.

For a further study, interaction effects among factors should be considered through a more standardized DOE, which will enhance the accuracy of experimental results.

NOMENCLATURE

u	velocity
η	melt viscosity
η_0	zero-shear-rate viscosity
ρ	density
$\dot{\varepsilon}$	shear strain rate
$\tilde{n}$	power-law index
τ^*	shear constant parameter in Cross-WLF model
τ_{ij}	deviatoric components of stress
δ_{ij}	Kronecker delta
σ_{ij}	stress tensor
$\xi(t)$	pseudo-time
ε_{ij}^d	deviatoric components of strain tensors
ε_m	spherical components of strain tensors
ε_{th}	thermal strain due to temperature changes
q^e	nodal displacements
r^e	nodal loads
t, t'	time variables
b_{1l}, b_{2l}, b_{3l}, b_{4l}, b_{1s}, b_{2s}, b_{3s}, b_{4s}, b_{3s}, b_{4s}, b_5, b_6, b_7, b_8, b_9	specific-volume model parameters
A_1,A_2	Cross-WLF model parameters
C_p	specific heat
D_1, D_2, D_3	Cross-WLF model parameters
G_1	bulk relaxation modulus

G_2	shear relaxation modulus
K	thermal conductivity
K^e	stiffness matrix
K^e_m	in-plane stiffness matrix
K^e_p	bending stiffness matrix
P	pressure
P_h	hydrostatic stress
T	temperature
T_g	crystallizing point
Trσ	trace of the stress tensor

References

1. Pomerleau, J.; Sanschagrin, B. Polym Eng Sci 2006, 46, 1275.
2. Jansen, K. M. B.; Pantani, R.; Titomanlio, G. Polym Eng Sci 1998, 38, 254.
3. Jansen, K. M. B.; Van Dijk, D. J.; Husselman, M. H. Polym Eng Sci 1998, 38, 838.
4. Yoshihara, N. J Polym Eng 2008, 28, 449.
5. Patel, P. SPE ANTEC 1997, 3632.
6. Kurt, M.; Kaynak, Y.; Kamber, O. S.; Mutlu, B.; Bakir, B.; Koklu, U. Int J Adv Manufact Technol 2010, 46, 571.
7. Guo, Z. Y.; Ruan, X. Y.; Peng, Y. H.; Li, D. Q. J Mater Eng Perform 2002, 11, 138.
8. De Santis, F.; Pantani, R.; Speranza, V.; Titomanlio, G. Ind Eng Chem Res 2010, 49, 2469.
9. Young, W. B.; Wang, J. Int Polym Proc 2002, 17, 271.
10. Shen, C. Y.; Li, H. M. Polym-Plast Technol Eng 2003, 42, 971.
11. Bushko, W.; Stokes, V. Polym Eng Sci 1995, 35, 365.
12. Choi, D.-S.; Im, Y.-T. Compos Struct 1999, 47, 655.
13. Kwon, K.; Isayev, A. I.; Kim, K. H.; Van Sweden, C. Polym Eng Sci 2006, 46, 712.
14. Kwon, K.; Isayev, A. I.; Kim, K. H. J Appl Polym Sci 2005, 98, 2300.
15. Kwon, K.; Isayev, A. I.; Kim, K. H. J Appl Polym Sci 2006, 102, 3526.
16. Kabanemi, K. K.; Vaillancourt, H.; Wang, H.; Salloum, G. Polym Eng Sci 1998, 38, 21.
17. Zhou, H. M.; Li, D. Q. Polym-Plast Technol Eng 2005, 44, 603.
18. Kramschuster, A.; Cavitt, R.; Ermer, D.; Chen, Z. B.; Turng, L. S. Polym Eng Sci 2005, 45, 1408.
19. Chang, T. C.; Faison, E, III. Polym Eng Sci 2001, 41, 703.
20. Wang, T. H.; Young, W. B.; Wang, J. Int Polym Proc 2002, 17, 146.
21. Postawa, P. Polimery 2005, 50, 201.
22. Liao, S. J.; Chang, D. Y.; Chen, H. J.; Tsou, L. S.; Ho, J. R.; Yau, H. T.; Hsieh, W. H.; Wang, J. T.; Su, Y. C. Polym Eng Sci 2004, 44, 917.
23. Bogucki, M.; Plaska, S.; Staczek, P. Polimery 2003, 48, 714.
24. Altan, M. Mater Des 2010, 31, 599.
25. Ozcelik, B.; Erzurumlu, T. J Mater Process Technol 2006, 171, 437.
26. Erzurumlu, T.; Ozcelik, B. Mater Des 2006, 27, 853.
27. Thomas, C. L.; Bur, A. J. Polym Eng Sci 1999, 39, 1619.
28. Jin, X. S.; Zhao, Z. F. SPE ANTEC 1998, 614.
29. Fan, Z.; Zheng, R.; Kennedy, P.; Yu, H.; Bakharev, A. SPE ANTEC 2000, 723.
30. Ozcelik, B.; Sonat, I. Mater Des 2009, 30, 367.
31. Ozcelik, B.; Erzurumlu, T. Int Commun Heat Mass Transf 2005, 32, 1085.
32. Liu, F.; Zhou, H. M.; Li, D. Q. J Reinf Plast Compos 2009, 28, 571.
33. Gu, Y. X.; Li, H. M.; Shen, C. Y. Adv Polym Tech 2001, 20, 14.
34. Shoemaker, J., Ed. Moldflow design guide: a resource for plastics engineers; Hanser Gardner Publications: Cincinnati, 2006.
35. Zhou, H.; Yan, B.; Zhang, Y. J Mater Process Technol 2008, 204, 475.
36. Zhou, H.; Li, D. Prog Nat Sci 2005, 15, 650.
37. Zhou, H.; Li, D. J Appl Polym Sci 2003, 90, 2377.
38. Ferry, J. D. Viscoelastic properties of polymers; John Wiley and Sons: Hoboken, 1980.
39. Zoetelief, W. F.; Douven, L. F. A.; Housz, A. J. I. Polym Eng Sci 1996, 36, 1886.
40. Felippa, C. CMAME 2003, 192, 2125.
41. Chen, W.; Cheung, Y. K. IJNME 2001, 51, 1259.
42. Zhou, H. M.; Xi, G. D.; Li, D. Q. Proc Inst Mech Engrs, Part C: J Mech Eng Sci 2006, 220, 573.
43. Huang, M. C.; Tai, C. C. J Mater Process Technol 2001, 110, 1.